Performance Evaluation of an Improved Double Intrinsic Layer CdTe/a-Si Thin Film Photovoltaic Cell

Muhammad Shahbaz Khan[1], Muhammad Owais Tariq[2], Safee Ullah[1], Muhammad Shahzad[1], and Talha Masood Khan[3]
[1] Dept. of Electrical Engineering, HITEC University, Taxila, Pakistan
[2] Dept. of Electrical Engineering, Pakistan Institute of Engineering and Technology, Multan, Pakistan
[3] Dept. of Civil, Materials and Environmental Engineering, University of Illinois at Chicago, Chicago, IL, USA
Email: {shahbaz.khan; safee.ullah; muhammad.shahzad}@hitecuni.edu.pk; engr.mot@gmail.com; tkhan41@uic.edu

***Abstract*—This paper presents a 1µm×1.25µm×1µm heterojunction thin film photovoltaic cell having "p-i1-i2-n" cell structure. The designed "ITO/p-CdTe/i1-CdTe/i2-a-Si/n-a-Si/ITO" photovoltaic cell is investigated, optimized and simulated in Silvaco TCAD. Finite Element Analysis (FEA) has been carried out to cater all physical and numerical models to generate practical results. For improvement in cell efficiency, a 1.52 eV wide-bandgap p-layer of CdTe is used which specifically improves the short circuit current (J_{SC}). J_{SC} is directly involved in the improvement of conversion efficiency. For the active region, an intrinsic CdTe layer is combined with an intrinsic amorphous silicon (a-Si) layer. This combination of intrinsic layers in active region is responsible for maximum absorption of photons with a wide range of energies and results in additional electron hole pair generation. Selective absorption is used to maximize light trapping and strong scattering of incident light into active region. Indium Tin Oxide (ITO) is used as front layer and back contact layer with Aluminum (Al) because it offers low resistivity of ~10^{-4} Ωcm and a transmittance of greater than 90%. Results have been validated by implementing two reported cells with p-i-i-n and p-i-n structures. The results indicate achievement of 28.05% conversion efficiency of the proposed heterojunction cell. The achieved efficiency is better than the efficiencies of the related cells compared in this work and also higher than that of the 25.6% of conventional Heterojunction Intrinsic Thin-film (HIT) silicon solar cells.**

***Index Terms*—Photovoltaic cell, p-i-i-n, heterojunction, solar cell, Silvaco TCAD**

I. Introduction

Since the dawn of economic development and industrialization, mankind has continuously been looking for different energy sources, as energy is a vital input for the technological advancement and economic development of any nation [1]. This rapidly growing energy demand led to the efforts in discovery of alternate and renewable energy sources to cope up the energy needs. Among various renewable energy sources, solar energy is rapidly becoming one of the most promising sources because of its abundant availability. Under the umbrella of solar research, "photovoltaics" is a promising technology to exploit solar energy, which actually converts sun light directly into electricity [2]. However, photovoltaic cells require efficient design solutions in terms of output efficiency and cost reduction to replace conventional energy sources completely. To enhance the performance of photovoltaic cells, various types of materials with different dimensions are exploited for harvesting solar energy [3], [4].

The progress in amorphous silicon (a-Si) cells has offered great flexibility in the manufacturing of various solar cell structures [5]. The efficiency of thin film solar cells is approaching about 23.4% (among all material types) based on NREL recent research-cell efficiency chart [6]. Amorphous silicon is considered to be a suitable material for thin film cells because absorption coefficient of amorphous silicon is similar to those found in direct band-gap semiconductors [7]. Copper Indium Gallium Selenide (CIGS) is also potential candidate of thin film technology. However in comparison, Cadmium Telluride (CdTe) is considered to be more efficient and cost-effective material in thin film technology with maximum recorded efficiency of 22.1% [6]. CdTe has a wide bandgap of 1.52 eV [8], hence it can efficiently convert light into electricity. The bandgap value of 1.52 eV corresponds to the bulk one at the room temperature (300 K). Moreover, it has a large absorption coefficient for light in visible spectrum because its bandgap is direct. This property makes it capable to absorb more than 90% of photons having energy greater than 1.52 eV even for a few µm thick layer size [5].

Several simulation tools have been reported to study the optical and electrical properties of solar cells, e.g., SCAP-1D, PC1D, Silvaco TCAD, etc. A CIGS cell has been investigated in [9] using the SCAP-1D simulation tool. The output parameters, e.g., short circuit current I_{SC}, open circuit voltage V_{OC}, and efficiency η have been investigated and optimized for the change in thickness of layers. Furthermore, a simulation study on CdS/CdTe

Manuscript received June 2, 2021; revised September 27, 2021; accepted October 5, 2021.
Corresponding author: Muhammad Shahbaz Khan (email: shahbaz.khan@hitecuni.edu.pk).

cells has been performed in [10] using the PC1D tool. The cells under study have been optimized based on the parameters like carrier lifetimes, thickness of absorber layers, doping concentrations, etc. In addition to the optimization in electrical and optical parameters, the geometrical parameters have also been in exploited in [11] using Silvaco TCAD simulation tool. Recently, a novel nano-pillar based CdS/CdTe cell has been in presented in [12] using Silvaco. The effect of Zn composition in the p-layer has been studied effectively using the Silvaco-Atlas software. Silvaco is an excellent tool to simulate the designed semiconductor devices and provides physically-based simulation results [13]. The physically-based simulators are preferred because they predict electrical and optical characteristics of the devices by exploiting and taking into consideration the specified practical/physical structures with bias conditions. It also applies various differential equations based on Maxwell's laws that simulate the important parameters, e.g., carrier transport, etc., through the designed solar cell.

In this work, a thin film heterojunction cell structure with layer hierarchy of "ITO/p-CdTe/i1-CdTe/i2-a-Si/n-a-Si/ITO" is proposed and implemented. The proposed cell structure is shown in Fig. 1, where i1 and i2 are the two intrinsic layers. Utilizing the beneficial properties of both CdTe and a-Si, the heterojunction cell structure proposed in this work is investigated, optimized and simulated using a commercially available semiconductor process and device simulation tool, i.e., Silvaco TCAD (Silvaco Inc., Santa Clara, CA, USA).

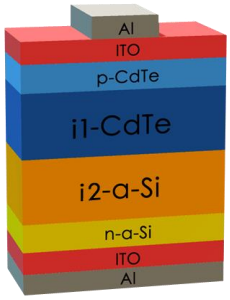

Fig. 1. The p-i1-i2-n heterojunction structure of the proposed photovoltaic cell (12-500-500-12 nm).

II. Design and Simulation

A. Cell Structure

Thin film cell structures are mostly preferred for manufacturing photovoltaic cells because of low manufacturing cost and the ease of large scale fabrication [14]. Furthermore, heterojunction solar cells having p-i-n structures with thin films of different materials offer more efficient utilization of the solar spectrum. Appropriate bandgaps in the intrinsic layer materials can result in the successful absorption and collection of photons with wide range of energies, resulting in additional electron hole pair generation [15].

The use of a wide bandgap absorber layer is quite useful while designing solar cells, even if non-conventional materials are being used [16]. For the efficient transmission of light into the absorber layer, a p-type layer with a wide bandgap is desirable [17]. When the photons enter the absorbing layer via p-type material having a wide bandgap, it enhances the short circuit current density. However, the extra wide bandgap in doping layers may result in a larger blocking barrier at the p-i interface which affects the conductivity. This conductivity reduction deteriorates the fill factor (FF), which is another important parameter responsible for a better conversion efficiency of a solar cell.

Among the choices for thin-film solar cells, CdTe is a promising option to deliver high conversion efficiency. Moreover, CdTe also exhibits impressive performance at very low light levels [18]. A point of concern with polycrystalline materials is the recombination at the grain boundaries. CdTe, due to having a short absorption length, minimizes this recombination. The reduction in recombination at grain boundaries, increases the generation of carriers within the depletion layer, which allows efficient collection of photons [19]. Taking all these reasons into account, CdTe was selected for the p-type layer in this research because the bandgap of CdTe is 1.52 eV at 300 K, which is sufficiently high value to be a wideband p-layer and not that high to cause high blocking barrier at the p-i interface.

CdTe was also considered to be the appropriate material for the i1 layer, which is the first intrinsic layer due to its high band gap. This high band gap of absorber layer is responsible for the efficient absorption of photons [16]. Hence, in this work, a-Si is chosen as the second intrinsic layer. The unabsorbed photons of i1 layer are absorbed in i2 layer for further electron hole pair generation and hence, increase the current density. Moreover, a-Si happens to be the most suitable material for manufacturing low cost photovoltaic cells. Thin films of a-Si can absorb sunlight efficiently due to its inherent disorder that is responsible for its high absorption coefficient, along with many other unique properties [20].

Normally n-CdTe layers are not preferred in thin film solar cells because they tend to increase the production/ manufacturing complexity. With the involvement of flexible electronics, this difficulty level has been further increased [21]. Therefore with p-type CdTe layer, use of other common n-type semiconductors is preferred [19]. For this reason, a-Si has been chosen for the bottom n-type layer as well.

For photovoltaic cells having adequate conversion efficiencies, it is important to achieve high current densities. The other important parameter responsible for a high current density is light trapping. Light trapping is extremely dependent on the quality of the transparent conductive oxide (TCO) used for electrodes. Due to the fact that near infrared region a-Si has low absorption coefficient, the parasitic absorption losses need to be minimized at the front and back electrodes for the optimum trapping of light. This is done by choosing a suitable TCO material for the front and back electrodes [22], [23]. Tin-doped indium-oxide, ITO is used in this

research as the top and bottom absorbing layers. This material boasts a low resistivity of up to $7.2\times10^{-4}\Omega$cm and a transmittance of greater than 90% [24].

For the selection of carrier lifetimes in CdTe regions, the values have been chosen on the basis of analyzing various numerical and experimental studies in literature that focus on the impact of carrier lifetimes on solar cell parameters. Carrier lifetimes are quite influential in determining the cell parameters, i.e., open circuit voltage V_{OC}, Short circuit current J_{SC} and the fill factor FF of solar cell [25], [26]. The carrier lifetimes directly impact the absorption of photons in the absorber layer of the solar cell and the absorption of photons can significantly increase a solar cell's efficiency [27]. The hole-density of CdTe, for over the past two decades, has been kept in a low range of ~10^{14} cm^{-3}. Recently, researchers have tried to increase the efficiency in CdTe cell by increasing the absorber doping-density and carrier lifetimes. Various studies have supported this recent trend and have reported enhancement in the V_{OC} and conversion efficiency by increasing the carrier density [28], [29] and lifetimes [28], [30], [31].

The impact of carrier density and carrier lifetime of CdTe on the performance of device has been evaluated in [28]. With the exception of the analysis on homojunction CdTe devices in [32], most of the modeling studies have limited themselves to $\tau \leq$ 10ns, for the value of hole-lifetime. This is why in [28], they could not improve the conversion efficiencies above 20%. The study reveals that to obtain a adequately high V_{OC} and an efficiency greater than 4% we need to use high values of hole-lifetime, i.e., $\tau >$ 10ns with doping ($p > 10^{16}cm^{-3}$) [28]. It has been observed that by increasing the hole-density and lifetime, an adequately high V_{OC} is obtained. This is why in our research, a hole-lifetime of 40 ns is used with the doping density in the order of $10^{19}cm^{-3}$.

In addition, an electron-lifetime of 10 ns, and donor-doping of order of 10^{14} cm^{-3} has also been analyzed in [28]. It was observed that it caused variation in carrier mobility and resulted in the decrement of cell efficiency by absolute 0.9%. Moreover, for the low electron lifetimes of $\tau <$ 1ns, significant decrement in J_{SC} had been observed. For the aforementioned reasons, in this research an electron-lifetime of 1ns has been used.

B. Device Simulation on Silvaco TCAD

To obtain the results of optical and electrical parameters of the proposed cell structure, finite element analysis (FEA) is carried out in Silvaco TCAD. This simulation tool solves various physical models i.e. Poisson equation, drift-diffusion current equation, Shockley-Read-Hall recombination (SRH), Auger recombination (AUGER), optical recombination (OPTR), parallel field mobility (FLDMOB) by dividing the whole structure into finite elements.

Besides, the photo-generation model which also utilizes a ray tracing algorithm, is used to calculate photo-generation, photon absorption and transmission in the material layers. For the evaluation of the proposed p-i1-i2-n cell, the air mass, AM 1.5 standard spectrum is used with an incident power density of 100mW/cm^2 in total.

The important device parameters e.g. the electrical, optical, mobility and recombination parameters are mentioned in Table I. While defining a material in the Atlas-Silvaco, there are some important parameters that need to be defined. These are defined by specifying the syntax functions for each parameter by using the MATERIAL statement, e.g., the bandgap (EG300), electron and hole density of states (NC300 and NV300), electron and hole motilities (MUN and MUP), etc.

TABLE I: IMPORTANT PARAMETERS USED FOR THE PROPOSED PHOTOVOLTAIC CELL.

Parameters	p-CdTe	i1-CdTe	i2-a-Si	n-a-Si
Layer thickness (nm)	12	500	500	12
Mobility gap (eV) [8]	1.52	1.52	1.86	1.8
Donor doping density (cm^{-3})	-	-	-	$1x10^{17}$
Acceptor doping density (cm^{-3})	5×10^{19}	-	-	-
Electron mobility (cm^2/Vs) [8], [33]	1100	1100	20	20
Hole mobility (cm^2/Vs)[8], [33]	80	80	4	4
Electron Life time (us) [33], [34]	0.001	0.001	0.01	0.01
Hole life time (us) [33], [34]	0.04	0.04	0.1	0.1
Activation energy (eV)[8], [33]	0.65-0.75	0.65-0.75	0.87	0.2
Electron Affinity (eV)	4.28	4.28	4.17	4.17
Characteristic energy (VB Tail) (eV) [33], [35]	0.65	0.65	0.05	0.05
Characteristic energy (CB Tail) (eV) [33] ,[35]	0.31	0.31	0.03	0.03

Materials like amorphous silicon have a plenty of defect states within their bandgap. Therefore, to accurately model such disordered materials, a continuous density of states has been used by mentioning CONTINUOUS in the DEFECTS statement. This statement helps to define the density of states as combination of Gaussian distribution of mid-gap states and the exponentially decaying band tail states. The model of density-of-states in Silvaco is composed of four bands, i.e., two deep level bands and two tail bands. The deep level bands include one 'acceptor-like' band and one 'donor-like' band. These deep level bands have been modeled using a Gaussian distribution. On the other hand, the two tail bands include a 'donor-like valence band' and an 'acceptor-like conduction band'. Furthermore, the density of states for the exponential tail distribution are described by its valence band and conduction band edge intercept densities, which are defined as NTD and NTA respectively. Similarly, the density of states for Gaussian distributions are described by its total density of states (NGA and NGD), its peak energy distribution (EGA and EGD), and its characteristic decay energy (WGA and WGD). All of the aforementioned values have been defined in the DEFECTS statement while modeling the density of states of amorphous silicon in Silvaco. The device simulated in Silvaco TCAD with embedded legend representing each layer separately is shown in Fig. 2, and the important SILVACO models used in this paper are tabulated in Table II.

TABLE II: IMPORTANT SILVACO MODELS FOR PARAMETERS USED IN THIS RESEARCH.

Parameter	SILVACO Model
Electron mobility	MUN
Hole mobility	MUP
Electron density of states	NC300
Holes density of states	NV300
Valence band edge intercept densities (Exponential Tail distribution)	NTD
Conduction band edge intercept densities (Exponential Tail distribution)	NTA
Total Density of States (Gaussian distribution)	NGA, NGD
Peak Energy Distribution (Gaussian distribution)	EGA, EGD
Characteristic Decay Energy (Gaussian distribution)	WGA, WGD
Energy Bandgap at 300K	EG300
Recombination (Shockley-Rea-Hall Model)	SRH
Direct Recombination Model	AUGER
Field Dependent Mobility	FLDMOB
Optical Recombination Model	OPTR
Fermi Statistics	FERMI
Donor doping density (cm-3)	REGION: DONOR
Acceptor doping density (cm-3)	REGION: ACCEPTOR
Electron Life time (us)	TAUN
Hole life time (us)	TAUP
Electron Affinity (eV)	MATERIAL: AFFINITY
Characteristic Energy	EV0.AMPHOTERIC

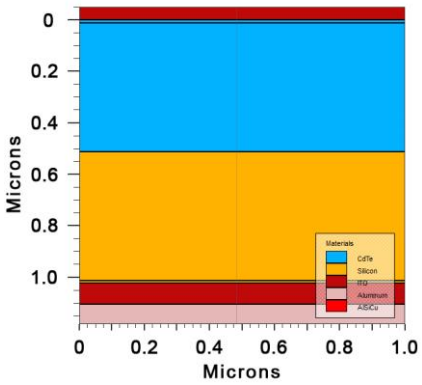

Fig. 2. Designed cell structure simulated in Silvaco TCAD.

The essential parameters to evaluate a solar cell's performance include the short circuit current (J_{SC}), open circuit voltage (V_{OC}), conversion efficiency (η), maximum power (P_m), and the fill factor (FF) [5]. The short circuit current of a photovoltaic cell is the current through the cell when the output is short circuited or in other terms the voltage across the cell is zero. The short-circuit current depends on a number of factors, i.e., the area of the solar cell, the number of photons, the spectrum of the incident light, the optical properties such as absorption and reflection, diffusion length and surface passivation. To remove its dependence on the area of the cell, it is more common to list the short circuit current density 'J_{SC}' (in mA/cm2), rather than the short circuit current 'I_{SC}'. In a photovoltaic cell that has a perfectly passivated surface and uniform generation, the equation for short circuit current density can be approximated as:

$$J_{SC} = qG\left(L_n + L_p\right) \tag{1}$$

where G is the generation rate, and L_n and L_p are the electron and hole diffusion lengths respectively and q is the charge in Coulombs. Even though (1) makes several assumptions but this equation in general means that the short circuit current density J_{SC} depends on two important parameters, i.e., the generation rate and the diffusion length.

The open circuit voltage, V_{OC} is considered as the maximum voltage which can be measured across a photovoltaic cell. The open circuit voltage is calculated by

$$V_{OC} = \frac{nkT}{q}\ln\left(\frac{I_L}{I_0}+1\right) \tag{2}$$

For a solar cell, the Fill Factor (FF) is a parameter that compares the maximum power of the cell with the theoretical power. It is the ratio of the actual highest achievable power. The value of short circuit current I_{SC} represents the maximum current, and the open circuit voltage V_{OC} is the maximum voltage from the solar cell. Yet, at both of these operating point values, the value of power P from the solar cell is zero. FF is a parameter that determines the maximum power from a solar cell by making use of the I_{SC} and V_{OC} values. The fill factor can be termed as the ratio of the maximum power from the solar cell to the product of V_{OC} and I_{SC} so that:

$$\mathrm{FF} = \frac{V_{MP}I_{MP}}{V_{OC}I_{SC}} \tag{3}$$

In the *I-V* curve of the V_{OC} and J_{SC}, the fill factor is actually the maximum covered area in the form of a square under the *I-V* curve.

The maximum power of a photovoltaic cell in terms of V_{OC}, J_{SC} and FF is calculated by

$$P_{max} = V_{OC}I_{SC}\mathrm{FF} \tag{4}$$

The efficiency (η) of a photovoltaic cell is defined as the ratio of the maximum output power to maximum input power. Efficiency is determined using (5):

$$\eta = \frac{V_{OC}I_{SC}\mathrm{FF}}{P_{in}} \tag{5}$$

III. RESULTS AND DISCUSSION

In the process of perfecting the solar cell proposed in this work, a number of layer thicknesses with variation of doping levels were simulated.

The i1 layer is tested from of 250nm to a layer size of 500nm and i2 layer is evaluated from 500nm to 1500nm. For the i1 layer, when the thickness is changed from 250nm to 500nm, the value of current density, J_{SC} increases from a value of 34.71mA/cm^2 to 40.79mA/cm^2. In a similar manner, the open circuit voltage, V_{OC} also increases from a value of 0.8537V to 0.8539V upon increasing the thickness of i1 layer from 250nm to 300nm but it starts dropping when thickness is further increased up till 500nm. The value of maximum power varies from 0.024W/cm^2 to 0.028W/cm^2 in an increasing manner, upon increasing the thickness of i1 layer from 250nm to 500 nm. With the same increase in thickness of the i1 layer, the conversion efficiency increases from 24.83% to 28.05%. Fig. 3 shows the variation of output parameters w.r.t variation in the thickness of i1 layer.

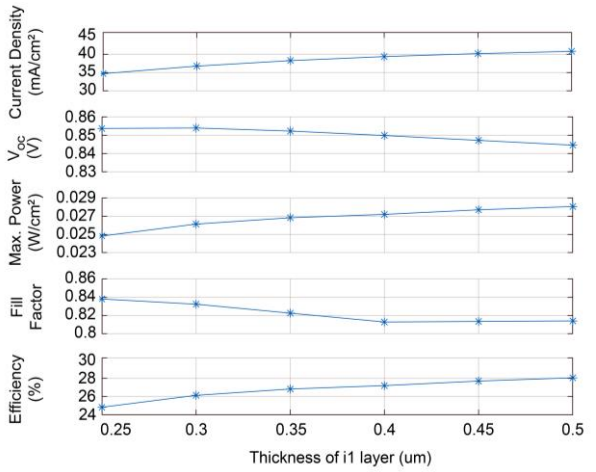

Fig. 3. Output parameters with the increase in thickness of i1 layer from 0.25 µm to 0.5 µm (250nm to 500nm).

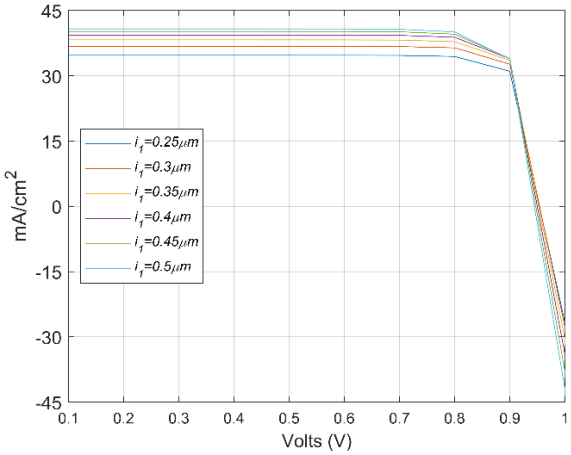

Fig. 4. Variation in the *I-V* curves of the proposed cell with change in thickness of i1 layer from 0.25 µm to 0.5 µm (250nm to 500nm).

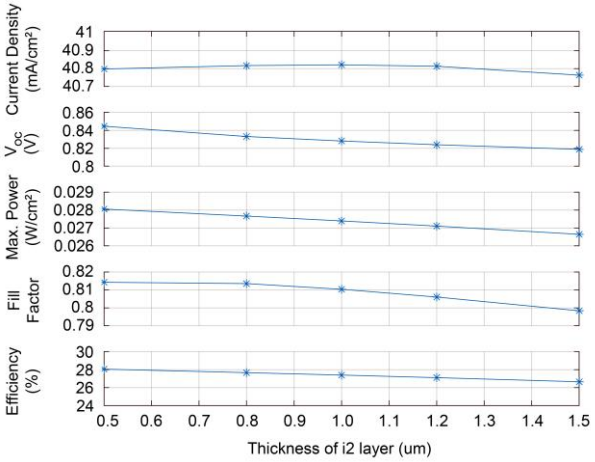

Fig. 5. Output parameters of the proposed cell with change in thickness of i2 layer from 0.5 µm to 1.5 µm (500nm to 1500nm).

The current-voltage characteristics or the *I-V* curves of the solar cell at different thicknesses of the i1 layer are presented in Fig. 4. It can be observed that the characteristic curve of the designed cell at 500nm, gives promising results in terms of improved values of J_{SC}, P_m and the conversion efficiency η. The improvement in J_{SC} and the efficiency η is due the fact that light is being absorbed more effectively [36].

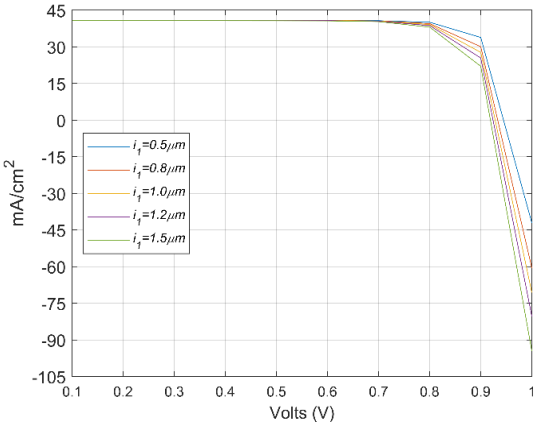

Fig. 6. Variation in the *I-V* curves of the proposed cell with change in thickness of i2 layer from 0.5 µm to 1.5 µm (500nm to 1500nm).

In addition, as we increase the thickness of intrinsic layer, the current starts reducing in spite of the low absorption coefficient. This happens because the electric field at the p/i interface starts reducing which results in the decrement of the intrinsic layer current collection. Fig. 5 shows that with the increase in thickness of i2 layer from 500nm to 1500nm, all parameters are decreased and the optimum values are obtained at 500nm. Therefore, the thickness of i2 layer has also been kept as 500nm. This can also be observed in the *I-V* curves of the cell with thickness of the i2 layer from 500nm to 1500nm in Fig. 6 that the highest curve is obtained at 500nm.

The thickness of i1 layer higher than 500nm had also been evaluated during the simulation and optimization process, i.e., for 600nm, 700nm and 800nm for the purpose of observing the effect of the increasing thickness on the output characteristics. No significant increase in the values of short circuit current (J_{SC}) was observed. However, the values of open circuit voltage (V_{OC}) continued to decrease. The decreasing pattern of V_{OC} wasn't that significant too but it caused deterioration in the *I-V* characteristics. Hence, the results for only the optimal range of thicknesses have been presented here for the ease of readers, depicting only those layer sizes which displayed significant increase or decrease in the output characteristics. However, for the values of i2 layer thickness lower than 500 nm, an improvement in values of open circuit voltages (V_{OC}) was observed but on the other hand, the values of short circuit current (J_{SC}) exhibited a decreasing pattern.

Doping concentration plays a pivotal role in defining the overall efficiency of a photovoltaic cell. A significant amount of light is absorbed at the top surface of the cell, which results in high carrier generation rate and high doping concentration in the absorber and window layers [10]. Our modeling showed that having 5×10^{19}cm^{-3} of acceptors in p-doped CdTe region and 1×10^{17}cm^{-3} donors in n-doped a-Si region provides optimal solar cell efficiency. The optimized layer sizes are given in the Table III. A constant doping profile was chosen in our case. Although, the increase in the doping concentration results in an increased built-in voltage and electric field, but it is increases the recombination rate and the

absorption coefficient of the p-layer. This increase in the aforementioned parameters, i.e., the recombination rate and the absorption coefficient reduces the generated current. Moreover, the short circuit current density Jsc gets saturated at larger doping concentrations, i.e., the concentrations values in the order of 10^{20} cm^{-3}. On the other hand, very low doping concentrations result in weaker electric field which in turn prevents the effective collection of photo carriers at the terminal.

TABLE III: SIZE OF THE OPTIMIZED LAYERS OF THE PROPOSED CELL STRUCTURE.

Layer Type	Size (μm)	Doping (cm^{-3})
ITO	0.07	-
P	0.012	$5e^{19}$
i-1	0.5	-
i-2	0.5	-
N	0.012	$1e^{17}$
ITO	0.08	-
Al (contact)	0.08	-

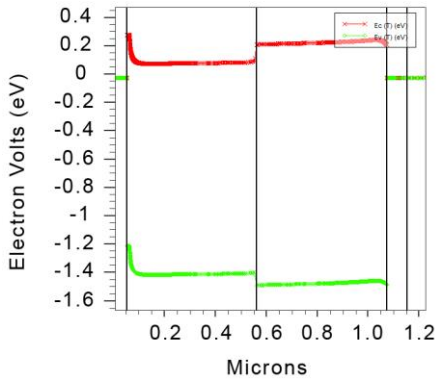

Fig. 7. The energy band diagram of the optimized cell.

The energy band diagram of the optimized cell using the optimized layer sizes mentioned in Table III is given in Fig. 7. EV represents the energy at the top of the valence band and EC represents the energy at the bottom of the conduction band.

Conduction and valence band offsets or discontinuities occurring at the junction are due to the difference in energy bandgaps of CdTe and a-Si. The results of output parameters of the cell with optimized layer sizes are given in Table IV. Short circuit current, an important factor responsible for better conversion efficiency of a solar cell, is the maximum current that follows from the solar cell. Fig. 8 shows the values of cathode current with respect to supply voltages.

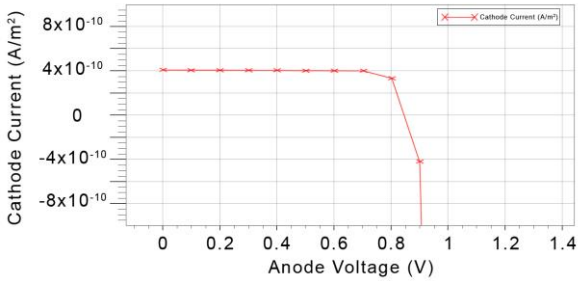

Fig. 8. Peak value of the short circuit current density of the proposed cell structure.

TABLE IV: OUTPUT PARAMETERS OF THE OPTIMIZED CELL

Output parameter	Value	Units
J_{sc}	00340.79	mA/cm^2
V_{oc}	0.84459	V
P_m	0.028	W/cm^2
FF	0.814	%
η	28.05	%

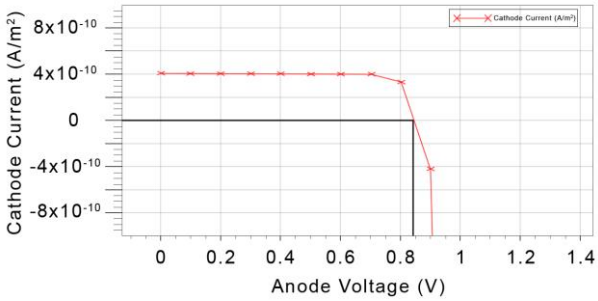

Fig. 9. Open circuit voltage of the cell structure where cathode current is zero.

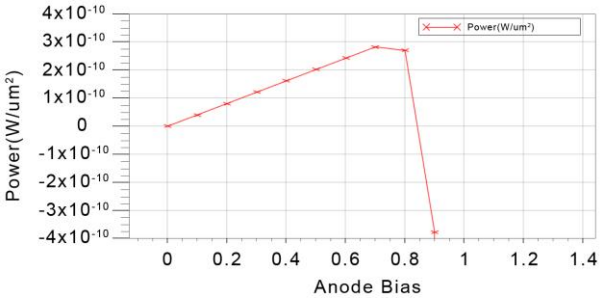

Fig. 10. Peak value of the maximum power, Pm of the proposed cell structure.

The other important parameter is the open circuit voltage and is measured at the point on the curve where total current corresponds to the zero crossing. Fig. 9 shows the value of open circuit voltage which can be seen to be 0.84459V at the zero crossing of the cathode current curve. The plot of the maximum power Pm of the designed cell is also shown in Fig. 10. The values given in Table IV can be verified through these plots.

In addition to the output parameters, other electrical properties of the cell have also been evaluated. The photo-generation model of Silvaco TCAD has been utilized which further runs a ray tracing algorithm. This algorithm determines the photo-generation and absorption of light in layers of photovoltaic cell. The ray tracing algorithm works by saving the combined effects of the transmission and reflection coefficients along with the losses occurring due to absorption. The variation in the photo-generation rate across the designed cell layers is shown in Fig. 11. It can be observed that the photo-generation rate is maximum at the p-i junction validating the choice of CdTe to be chosen as p and i1 layers. The increase in the short circuit current density J_{SC} and FF plays an essential role in the enhancement of the efficiency η as they are responsible for more electron-hole pairs which in turn contribute in producing the photogenerated current. On the other hand, in case of a small absorber thickness, light is crudely absorbed and therefore it almost appears transparent to that wavelength. Speaking of extremely large thickness values, the Jsc undergoes saturation and it happens to be one of the important reasons of efficiency saturation.

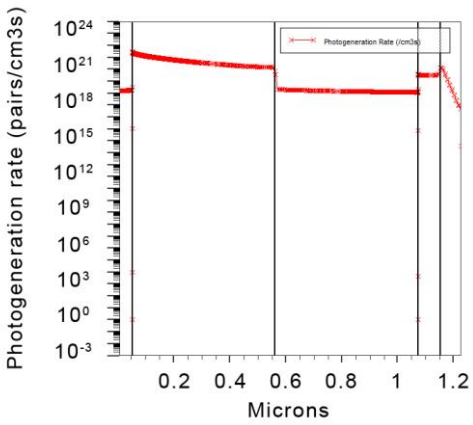

Fig. 11. The photogeneration rate of the designed cell depicting the pattern and the peak value.

The electric field at the p/i interface of the photovoltaic cell needs to be kept maximum to collect large number of electron hole pairs (EHPs) that are generated due to the absorption of photons. However, with the increase in the electric field, the recombination rate also increases and this additional increase in the recombination rate may result in low efficiency of the cell. Hence, a trade-off has to be done between the electric field and the rate at which recombination occurs. This compromise can be observed at the p/i interface of the designed photovoltaic cell in Fig. 12 and Fig. 13 which depict the plots of photon absorption and recombination rate respectively.

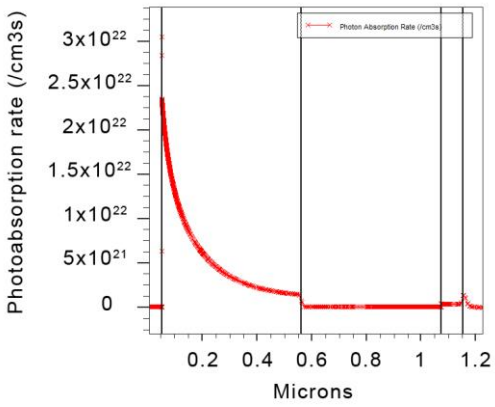

Fig. 12. Photoabsorption rate of the designed cell depicting the pattern and the peak value.

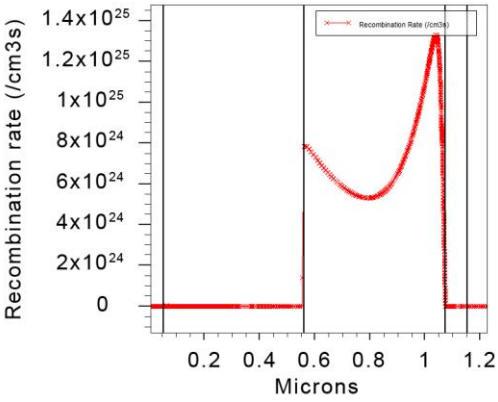

Fig. 13. Recombination rate of the designed cell depicting the pattern and the peak value.

TABLE V. PEAK VALUES OF THE PHOTOGENERATION, ABSORPTION AND RECOMBINATION RATE

Rate (/cm^{3}s)	Value
Peak photo-generation	2×10^{22}
Peak photon absorption	3.15×10^{22}
Peak recombination	133×10^{25}

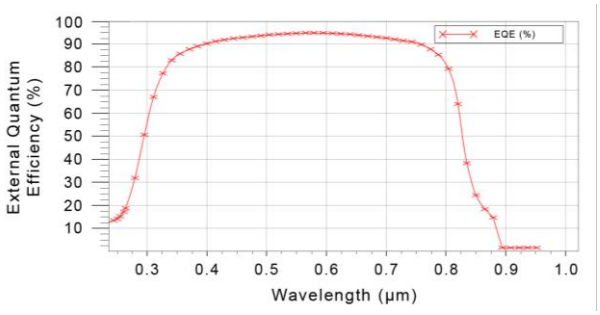

Fig. 14. The External Quantum Efficiency (EQE) behavior of the designed photovoltaic cell w.r.t the wavelength.

The selection of wide bandgap materials for p and i-1 layers, increases the absorption of incident photons. This can be observed in Fig. 12 that the maximum absorption rate is evident at the p-i interface of the cell.

It is worthwhile to analyze the generation-recombination phenomenon in a photovoltaic cell because the distribution of carrier generation and recombination directly affect the distribution of the trapped charge. The net rate of the 'electron capture' from the conduction band and the 'hole capture' from the valence band are calculated and are plotted as the recombination rate at output. The peak values of photogeneration, absorption and recombination rate are given in Table V.

Furthermore, it is quite essential to observe how the designed photovoltaic cell responds to the solar spectrum. Therefore, to measure the optical performance of the designed cell more effectively, the external quantum efficiency (EQE) is plotted. External quantum efficiency is actually the ratio of the available photocurrent and the source photocurrent. Fig. 14 shows the simulated EQE of the designed cell under AM1.5G illumination in the wavelength range of 200nm to 1000nm. It can be observed that the maximum absorption region the designed photovoltaic cell expands between the ranges of 350nm to 800nm with an average EQE of 94%.

Speaking of the experimental CdTe photovoltaic cells in literature, the latest highly optimized CdTe cells have attained efficiencies of 22.1% for small area devices and 18.6% for photovoltaic modules [37]. A recent experimental study [38], incorporates a CdSe layer with a thin CdS layer for the optimization of CdTe solar cells. Several cell structures have been fabricated and tested by the authors. A highest cell efficiency of 17.8% has been achieved. Furthermore, considering the latest experimental/actual state of the art realizations of CdTe cells, a ZnSe/CdTe solar cell is fabricated in [39] that highlights the role of ZnSe layer in improving the performance of fabricated CdTe cell.

Moreover, by utilizing various improved designs and majorly removing CdS from these design, an eminent improvement has been observed in last 5 years. The new designs, apart from experimenting new materials other

than CdS, exploit the new features, e.g., copper embedding, band gap grading, and improved transparent n-layers. With the aforementioned changes, manufacturers like 'First Solar' have produced devices offering 21.5% to 22.1% efficiencies. When compared to these latest reported solar cells, the proposed and simulated cell in our research outperforms the aforementioned experimental cells.

IV. Comparison with the p-i-i-n (a-Si/μC-Si) and the p-i-n (CdTe/CdS) Solar Cells

Two other solar cells, i.e., a p-i-i-n solar cell having layer hierarchy as "p-a-Si/i1-a-Si/i2-μC-Si/n- μC" [33] and a p-i-n solar cell with cell structure "p-CdTe/i-CdTe/n-CdS" [40] are also simulated. Both cells are simulated as per the dimensions and material properties mentioned in their published work. The comparison of results of output parameters is given in Table VI. It can be seen that the designed cell has the higher short circuit current value with a lower V_{OC} but due to the improved short circuit current and the maximum power, the conversion efficiency is also improved.

The *I-V* curves for the cells to be compared have also been generated on Silvaco TCAD and compared with the solar cell designed in this study. The comparison is given in Fig. 15. The *I-V* curves and the results in Table VI clearly indicate that the conversion efficiency of the proposed p-i1-i2-n cell simulated in this study is higher than the other two solar cells. This is due to the large bandgap of the i1-CdTe layer and also because light is absorbed more effectively by both the i1 and i2 layers. This efficient absorption tends to generate of more electron hole pairs (EHPs) and the carriers which improve the current density of the cell. The increase in J_{SC} is evident from the comparison of the results given in Table VI.

Table VI: Comparison of Results of Output Parameters of the Proposed Cell, the Cell in [33] and the Cell in [40].

Output Parameters	Chang [33]	Hossain [40]	This Study (p-i1-i2-n Solar Cell.)
J_{sc} (mA/cm^2)	9.2018	27.29	40.79
V_{oc} (V)	0.916	1.10	0.84459
FF	0.83	0.89	0.814
η (%)	8.73	26.74	28.05

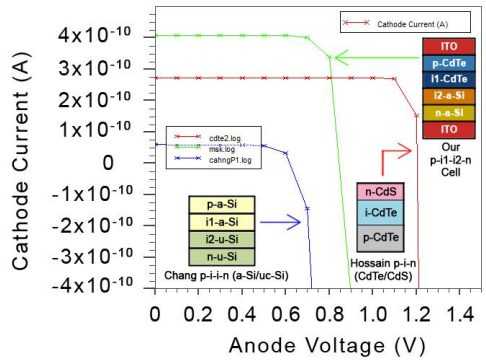

Fig. 15. Comparison of the *I-V* curves of the proposed cell simulated in this study (green), the p-i-i-n cell in [33] (blue) and the p-i-n cell in [40] (red).

V. Conclusion

In this study, a heterojunction thin film photovoltaic cell has been designed, optimized and simulated. The designed cell has a double intrinsic layer making the structure of cell to be p-i1-i2-n. The layer hierarchy as per the material selection is "ITO/p-CdTe/i1-CdTe/i2-a-Si/n-a-Si/ITO". The double intrinsic layer used in this research proved to be a good photon absorber. The materials chosen for i1 and i2 layers are CdTe and a-Si respectively. This combination of intrinsic layers in active region is responsible for maximum absorption of photons with a wide range of energies and results in additional electron hole pair generation. For the p-type layer, CdTe was chosen due its property of having a wide bandgap. For the n-type layer, a-Si is considered. The improvement in the results of electrical and optical parameters of the proposed cell indicates the advantage of optimizing the thickness of i1-CdTe and the i2-a-S layers. To maximize light trapping and strong scattering of incident light into active region, ITO is used as front layer and back contact layer with Aluminum because it offers low resistivity of ~10^{-4} Ωcm and a transmittance of greater than 90%. The results indicate achievement of 28.05% efficiency of the designed thin film cell which is higher than the compared solar cells of similar or related reported cell structures.

Conflict of Interest

The authors declare no conflict of interest.

Author Contributions

Conceptualization and simulation of the designed cell is performed by Muhammad Shahbaz Khan. Simulation of the cells to be compared and analytical validation is carried out by Muhammad Owais Tariq. Conduct of literature review and the article draft is written by Safee Ullah and Muhammad Shahzad. Supervision and material selection for layers and optimization of the designed cell is done by Talha Masood Khan. All authors had approved the final version of this paper.

References

[1] R. M. Elavarasan, S. Afridhis, R. R. Vijayaraghavan, U. Subramaniam, and M. Nurunnabi, "SWOT analysis: A framework for comprehensive evaluation of drivers and barriers for renewable energy development in significant countries," *Energy Reports*, vol. 6, pp. 1838-1864, Nov. 2020.

[2] S. Sivasubramaniam, A. Faramus, R. D. Tilley, and M. M. Alkaisi, "Performance enhancement in silicon solar cell by inverted nanopyramid texturing and silicon quantum dots coating," *Journal of Renewable and Sustainable Energy*, vol. 6, no. 1, p. 011204, 2014.

[3] G. Grancini and M. K. Nazeeruddin, "Dimensional tailoring of hybrid perovskites for photovoltaics," *Nature Reviews Materials*, vol. 4, no. 1, pp. 4-22, 2019.

[4] O. Inganäs, "Organic photovoltaics over three decades," *Advanced Materials*, vol. 30, no. 35, p. 1800388, 2018.

[5] M. D. Archer and R. Hill, *Clean Electricity from Photovoltaics*, World Scientific, 2001.

[6] NREL. Best Research-Cell Efficiency Chart. The National Renewable Energy Laboratory, Golden, Colorado, USA. [Online]. Available: https://www.nrel.gov/pv/cell-efficiency.html

[7] R. W. Miles, "Photovoltaic solar cells: Choice of materials and production methods," *Vacuum*, vol. 80, no. 10, pp. 1090-1097, 2006.

[8] A. J. Strauss, "The physical properties of cadmium telluride," *Rev. Phys. Appl. (Paris)*, vol. 12, pp. 167-184, Feb. 1977.

[9] S. Tobbeche and H. Amar, "Two-dimensional Modelling and Simulation of CIGS thin-film solar cell," *Journal of New Technology and Materials*, vol. 4, no. 1, pp. 89-93, May. 2014.

[10] D. K. Shah, D. Kc, M. Muddassir, M. S. Akhtar, C. Y. Kim, and O. B. Yang, "A simulation approach for investigating the performances of cadmium telluride solar cells using doping concentrations, carrier lifetimes, thickness of layers, and band gaps," *Solar Energy*, vol. 216, pp. 259-265, Mar. 2021.

[11] I. E. Tinedert, F. Pezzimenti, M. L. Megherbi, and A. Saadoune, "Design and simulation of a high efficiency CdS/CdTe solar cell," *Optik*, vol. 208, p. 164112, 2020.

[12] D. K. Sharma, N. S. K, M. S. Ilango, and S. K. Ramasesha, "Efficiency enhancement of the CdS/CdTe solar nanostructured cell using electron-reflecting layer," *IEEE Trans. on Electron Devices*, vol. 68, no. 3, pp. 1129-1134, 2021.

[13] I. E. Tinedert, A. Saadoune, I. Bouchama, and M. A. Saeed, "Numerical modelling and optimization of CdS/CdTe solar cell with incorporation of Cu2O HT-EBL layer," *Optical Materials*, vol. 106, p. 109970, 2020.

[14] Y. Zhang, S. W. Ng, X. Lu, and Z. Zheng, "Solution-processed transparent electrodes for emerging thin-film solar cells," *Chemical Reviews*, vol. 120, no. 4, pp. 2049-2122, 2020.

[15] M. Konagai, "Present status and future prospects of silicon thin-film solar cells," *Japanese Journal of Applied Physics*, vol. 50, p. 030001, 2011.

[16] A. Crovetto, R. Nielsen, E. Stamate, *et al.*, "Wide band gap Cu2SrSnS4 solar cells from oxide precursors," *ACS Applied Energy Materials*, vol. 2, no. 10, pp. 7340-7344, 2019.

[17] Y. Tawada, H. Okamoto, and Y. Hamakawa, "a - SiC:H/a - Si:H heterojunction solar cell having more than 7.1% conversion efficiency," *Applied Physics Letters*, vol. 39, no. 3, pp. 237-239, 1981.

[18] I. Mathews, S. N. R. Kantareddy, Z. Liu, *et al.*, "Analysis of CdTe photovoltaic cells for ambient light energy harvesting," *Journal of Physics D: Applied Physics*, vol. 53, no. 40, p. 405501, 2020.

[19] J. Britt and C. Ferekides, "Thin-film CdS/CdTe solar cell with 15.8% efficiency," *Applied Physics Letters*, vol. 62, no. 22, pp. 2851-2852, 1993.

[20] S. Guha, "Thin film silicon solar cells grown near the edge of amorphous to microcrystalline transition," *Solar Energy*, vol. 77, no. 6, pp. 887-892, 2004.

[21] J. Ramanujam, D. M. Bishop, T. K. Todorov, *et al.*, "Flexible CIGS, CdTe and a-Si:H based thin film solar cells: A review," *Progress in Materials Science*, vol. 110, p. 100619, 2020.

[22] M. Berginski, J. Hüpkes, A. Gordijn, *et al.*, "Experimental studies and limitations of the light trapping and optical losses in microcrystalline silicon solar cells," *Solar Energy Materials and Solar Cells*, vol. 92, no. 9, pp. 1037-1042, 2008.

[23] X. D. Zhang, Y. Zhao, Y. T. Gao, *et al.*, "Influence of front electrode and back reflector electrode on the performances of microcrystalline silicon solar cells," *Journal of Non-Crystalline Solids*, vol. 352, no. 9, pp. 1863-1867, 2006.

[24] Z. Chen, W. Li, R. Li, Y. Zhang, G. Xu, and H. Cheng, "Fabrication of highly transparent and conductive indium–tin oxide thin films with a high figure of merit via solution processing," *Langmuir*, vol. 29, no. 45, pp. 13836-13842, 2013.

[25] J. Sites and J. Pan, "Strategies to increase CdTe solar-cell voltage," *Thin Solid Films*, vol. 515, no. 15, pp. 6099-6102, 2007.

[26] A. Kanevce and T. A. Gessert, "Optimizing CdTe solar cell performance; Impact of variations in minority carrier lifetime and carrier density profile," in *Proc. 37th IEEE Photovoltaic Specialists Conf.*, 2011, pp. 000153-000153.

[27] G. Fonthal, L. Tirado-Mejía, J. I. Marín-Hurtado, H. Ariza-Calderón, and J. G. Mendoza-Alvarez, "Temperature dependence of the band gap energy of crystalline CdTe," *Journal of Physics and Chemistry of Solids*, vol. 61, no. 4, pp. 579-583, 2000.

[28] A. Kanevce, M. O. Reese, T. M. Barnes, S. A. Jensen, and W. K. Metzger, "The roles of carrier concentration and interface, bulk, and grain-boundary recombination for 25% efficient CdTe solar cells," *Journal of Applied Physics*, vol. 121, no. 21, p. 214506, 2017.

[29] J. M. Burst, J. N. Duenow, D. S. Albin, *et al.*, "CdTe solar cells with open-circuit voltage breaking the 1 V barrier," *Nature Energy*, vol. 1, no. 3, pp. 1-8, 2016.

[30] M. Gloeckler, I. Sankin, and Z. Zhao, "CdTe solar cells at the threshold to 20% efficiency," *IEEE Journal of Photovoltaics*, vol. 3, no. 4, pp. 1389-1393, 2013.

[31] D. Kuciauskas, P. Dippo, Z. Zhao, *et al.*, "Recombination analysis in cadmium telluride photovoltaic solar cells with photoluminescence spectroscopy," *IEEE Journal of Photovoltaics*, vol. 6, no. 1, pp. 313-318, 2016.

[32] T. Song, A. Kanevce, and J. R. Sites, "Exploring the potential for high-quality epitaxial CdTe solar cells," in *Proc. IEEE 40th Photovoltaic Specialist Conf. (PVSC)*, 2014, pp. 2412-2415.

[33] W. R. Chang, J. T. Lin, Y. C. Eng, *et al.*, "Simulation of a novel single junction thin film solar cell," in *Proc. International Symposium on Next-Generation Electronics*, 2013, pp. 469-472.

[34] J. W. Mayer, "Evaluation of CdTe by nuclear particle measurements," *Journal of Applied Physics*, vol. 38, no. 1, pp. 296-301, 1967.

[35] S. G. Kumar and K. S. R. K. Rao, "Physics and chemistry of CdTe/CdS thin film heterojunction photovoltaic devices: fundamental and critical aspects," *Energy & Environmental Science*, vol. 7, no. 1, pp. 45-102, 2014.

[36] Y. Poissant, P. Chatterjee, and P. R. i. Cabarrocas, "Analysis and optimization of the performance of polymorphous silicon solar cells: Experimental characterization and computer modeling," *Journal of Applied Physics*, vol. 94, no. 11, pp. 7305-7316, 2003.

[37] M. Green, E. Dunlop, J. Hohl-Ebinger, M. Yoshita, N. Kopidakis, and X. Hao, "Solar cell efficiency tables (version 57)," *Progress in Photovoltaics: Research and Applications*, vol. 29, no. 1, pp. 3-15, 2021.

[38] C. Li, G. Hu, X. Hao, C. Li, *et al.*, "Performance improvement of CdS/CdTe solar cells by incorporation of CdSe layers," *Journal of Materials Science: Materials in Electronics*, vol. 32, no. 14, pp. 19083-19094, 2021.

[39] H. I. Elsaeedy, A. A. Hassan, H. A. Yakout, and A. Qasem, "The significant role of ZnSe layer thickness in optimizing the performance of ZnSe/CdTe solar cell for optoelectronic applications," *Optics & Laser Technology*, vol. 141, p. 107139, 2021.

[40] M. M. Hossain, M. M. U. Karim, S. Banik, N. A. Jahan, and M. A. Matin, "Design of a high efficiency ultrathin CdTe/CdS p-i-n solar cell with optimized thickness and doping density of different layers," in *Proc. International Conf. on Advances in Electrical, Electronic and Systems Engineering (ICAEES)*, 2016, pp. 305-308.

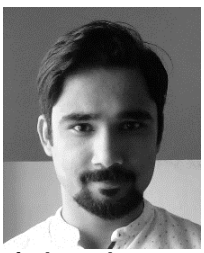

Muhammad Shahbaz Khan received the B.S. degree in Electronics Engineering from NFC Institute of Engineering and Technology, Multan, Pakistan in 2011 and the M.S. degree in Electrical Engineering (Photovoltaics) from HITEC University, Taxila, Pakistan in 2015. He is currently pursuing a Ph.D. degree in Electrical Engineering with Riphah International University, Islamabad, Pakistan. He is currently a Lecturer at the Department of Electrical Engineering, HITEC University, Taxila, Pakistan. His research interests include Photovoltaics, MEMS sensors and actuators, Bio-MEMS, and microfabrication

Muhammad Owais Tariq received the BSc Electronics Engineering degree from NFC Institute of Engineering and Technology, Multan in 2011, and an MS degree in Electrical Engineering (Photovoltaics) from College of Electrical and Mechanical Engineering (CEME), NUST, Islamabad, Pakistan. He is currently pursuing a Ph.D. degree in Electrical Engineering at Riphah International University, Islamabad, Pakistan. His research interest includes microelectromechanical device designing for biomedical and pharmaceutical applications. He is currently working as Assistant Professor at the Pakistan Institute of Engineering and Technology, Multan, Pakistan.

Safee Ullah received the BS Electronics Engineering degree from Wah Engineering College, Wah, Pakistan in 2011, and an MS degree in Electrical Engineering from HITEC University, Taxila, Pakistan in 2017. He is currently pursuing a Ph.D. degree in Electrical Engineering at HITEC University, Taxila, Pakistan, where is also serving as a Lecturer. His research interests include model order reduction of high order systems.

Muhammad Shahzad received his BS and MS degrees in Electrical Engineering from HITEC University Taxila, Pakistan in 2011 and 2015 respectively. He is currently enrolled in PhD in Electrical Engineering at HITEC University. He is currently working as a lecturer in HITEC University Taxila, Pakistan. His research interests are power systems and artificial intelligence.

Talha Masood Khan received his M.S and B.S degrees in Electrical and Electronics Engineering from National University of Sciences and Technology (NUST), Islamabad, Pakistan and Bahauddin Zakariya University, Multan, Pakistan in 2013 and 2011 respectively. He received his Ph.D. degree from Bilkent University, Ankara, Turkey in 2020, majoring in MEMS, acoustics, and nanotechnology. From 2013 to 2014 he was with the Department of Electrical Engineering, PIET, Multan, Pakistan, as a University Lecturer and was also a visiting Lecturer at Dept. of Physics, Bahauddin Zakariya University. From 2014 to 2020 he was a Graduate Research and Teaching Assistant with UNAM, Bilkent University. In 2021 he joined the University of Illinois at Chicago as a Postdoctoral Research Associate at the College of Engineering. His research interests include MEMS sensors and actuators, airborne acoustics, non-destructive evaluation and ultrasonic transducer design (CMUT).